IEEE Access
Multidisciplinary | Rapid Review | Open Access Journal

Received January 19, 2021, accepted March 11, 2021, date of publication March 17, 2021, date of current version March 25, 2021.

Digital Object Identifier 10.1109/ACCESS.2021.3066445

Moon Impact Crater Detection Using Nested Attention Mechanism Based UNet++

YUTONG JIA, LEI LIU, AND CHENYANG ZHANG
Department of Surveying and Mapping and Space Environment, Space Engineering University, Beijing 101407, China
Corresponding author: Yutong Jia (hgdjyt@163.com)

ABSTRACT Impact craters are the most prominent topographic feature on the lunar surface, which will play a significant role in constructing lunar bases and lunar surface activities in the future. Traditional meteorite crater recognition methods are mainly based on artificial interpretation, usually combined with classical image processing methods. However, due to the different diameters and shapes of impact craters, the traditional crater identification methods have significant errors and low efficiency for small or overlapping impact craters. This paper proposes an automated algorithm termed nested attention-aware U-Net (NAU-Net) for crater detection using a lunar's digital elevation model (DEM). It then uses template matching to effectively calculate the longitude, latitude, and radius of the crater. It is worth mentioning that NAU-Net is primarily based on UNet++ and attention networks and applies a sequence of nested dense convolution blocks, preferably of classical convolution, which combines U-Net++ and Attention Gates advantages. Since our network uses nested intensive attentional aware connections and in-depth supervision, the training process of the NAU-Net is simple, which can achieve more accurate detection and recognition. In fact, the network can recognize smaller or overlapping impact craters and larger and more complex ones. In honor of lunar impact craters, compared with U-Net, UNet++, Dense-Unet, Attention-Unet, R2-Unet, our model achieved recall rates and accuracy of 0.791 and 0.856, better than other improved U-Net models. The experimental results show that the NAU-Net model can be used to extract impact craters.

INDEX TERMS Crater recognition, dense convolution block, deep supervision, nested attention-aware U-Net, template matching.

I. INTRODUCTION

Impact craters are the various significant landform of the lunar covering [1]. They are gradually formed by the impact of meteorites by satellites, giant asteroids, or other stars. There are numerous and different impact craters, showing annular pit structures of different sizes and uneven aggregation. The study of the morphology of lunar impact craters helps in-depth understanding of planets' morphology and evolution. It assists in the exploration of planetary geology and mineral resources. For example, impact crater size distributions and spatial statistics can infer the relative geological ages and surface properties of the planet's surface [2]. By observing the morphology and spatial distribution of impact craters, we can infer the time sequence and location of geological events on the planet's surface in the past [3]. The existence of water ice can be inferred by measuring the dielectric constant of an impact crater. Secondly, the identification of impact crater is also used for spacecraft navigation and landing obstacle avoidance [4].

Since the beginning of lunar exploration, the accurate and rapid identification of impact craters has always focused on in-depth space exploration. Many researchers have also proposed a series of lunar surface impact craters extraction algorithms. According to the different design ideas of these algorithms, their development can be roughly divided into two directions: the traditional algorithm that uses image processing technology to identify impact craters [5], [6] and the intelligent algorithm that introduces a deep learning model to extract impact craters [7]–[10].

The early artificial recognition method is suitable for the impact crater recognition of image data. The accuracy of the craters depends on the judge reader's prior knowledge, and the recognition efficiency is low, so many reliable methods are created to automatically extract the impact crater. Among them, the methods based on morphology fitting include Hough transform [6], [11], conic curve fitting [12], template matching [13], and other algorithms [14]. Flores-Méndez [6]

The associate editor coordinating the review of this manuscript and approving it for publication was Guitao Cao.

and Michael [11] used Hough transform to analyze and process MOLA data, and the latter obtained more than 75% impact craters with a diameter higher than 10 km. The advantage of fuzzy Hough transform is to search the data point set with a high fitting degree, which can effectively reduce the error boundary obtained by traditional Hough transform. Alejandro Flores-Méndez [6] proposed a Sliding Window Hough Transform (HTSW) to improve the identification rate of incomplete impact craters or shape-damaged impact craters. Kim *et al.* [5] used the least square fitting method (DLS) proposed by Fitzgibbon [12], the optimal valuation fitting method (OE) proposed by [15], and the ring algorithm based on the regression formula proposed by [16] to identify the Mars impact crater. By comparing the Hough ring transform algorithm's recognition results, the conic curve fitting method has higher reliability and a more vital ability to overcome the influence of interference noise. The least-square fitting way is more suitable for the marginal tissue. Burl [13] used Continuously Scalable Template Matching to test Clementin sea data and correctly identified 80% impact craters with a diameter of more than 4 pixels, with a misclassification rate of 12%. At the same time, Vinogradova *et al.* [17] used this method to conduct experiments on the Mars Orbiter Camera data and correctly identified 88% of the impact craters in the selected survey area.

The traditional crater recognition algorithm relies on the construction and matching of data quality and crater features. Its core idea is to build a more accurate crater feature model and a more efficient template matching algorithm. However, due to a wide variety of geomorphological features of impact craters, nesting and overlapping of impact craters in the same area, as well as the insufficient number of data samples of impact craters and the low level of feature abstraction, the development of traditional identification algorithms have encountered bottlenecks.

Lately, deep learning has attained a significant victory in the area of computer vision. The algorithm primarily based on a convolutional neural network (CNN) can better solve target detection, image segmentation, and image classification. Meteorite crater identification can also be converted into meteorite crater detection and segmentation in image data.

For the classification of meteorite craters, Cohen and Ding [18] proposed a meteorite craters detection and classification algorithm based on a genetic algorithm. Fa and Jin [19] proposed a neural network method to automatically detect and classify meteorite craters. Silburt *et al.* [7] based on the U-Net model of image semantic segmentation in deep learning, proposed a lunar surface impact crater recognition model, and transferred the model to the surface of Mercury impact crater recognition, and achieved good results. Lee *et al.* [8] extended this model structure to impact craters on the surface of Mars and then proposed the DeepMars model to realize the rapid identification of impact craters on the surface of Mars. Wang *et al.* [20] optimized the model, combined with a residual network, and proposed an effective residual U-Net (ERU-Net), which achieved good results in the test.

Compared with the traditional impact crater identification methods, the deep learning-based impact crater identification method can better solve significant radius differences and complex morphological characteristics of an impact crater. However, since most deep learning models are UNet models, they have a low ability to identify small or overlapping impact craters with low accuracy and lack of objective evaluation criteria. Therefore, this paper takes lunar surface impact craters as the research object, builds an intelligent identification framework of lunar surface impact craters based on NAU-Net, and introduces nested attention connection modules and deep supervision to improve detection accuracy. Besides, more proper extraction and post-processing operations also enable the detection model to reduce false-negative errors effectively.

This paper's relaxation is prepared as follows: Sections II presents a brief overview of the related work. In Section III, we will introduce the essential points of the proposed NAU-Net. Section IV describes the experimental statistics and results. Section V presents the discussion. Finally, in part VI, we will summarize our work and furnish an outlook for future work.

II. RELATED WORK

This section briefly introduces semantic segmentation and two deep mastering techniques: nested dense connection and attention gates.

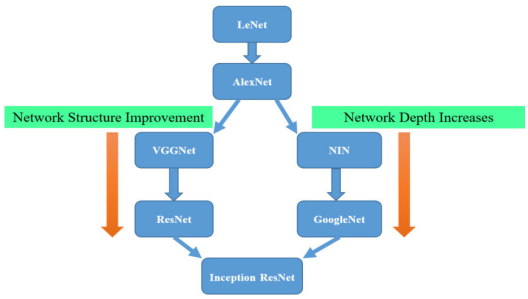

FIGURE 1. Evolutionary of convolutional neural network.

A. SEMANTIC SEGMENTATION STRUCTURE

The history of the structural evolution of CNN is shown in Fig. 1. The first CNN model was created in 1989, followed by LeNet in 1998. With the introduction of ReLu and Droout and GPU's historic opportunities and big data, CNN had a historic breakthrough in 2012. After 2012, the evolution path of CNN can be summarized as four:

1) Deeper networks.
2) Enhance the function of the convolutional module and the integration of the above two ideas.
3) From classification to detection.
4) Add new functional modules.

In 2014, Long *et al.* [21] presented the Fully Convolutional Neural Network (FCN), which leaped forward in semantic

segmentation, genuinely opening the pixel-level semantic segmentation network. FCN is improved based on the CNN classification network, and the complete connection layer in CNN is changed by the convolutional layer to establish the fully convolutional network. FCN proposed the encoder-decoder architecture based on CNN, which proved that the semantic segmentation network was trained end-to-end on the image of variable size. A better semantic segmentation network was obtained by continuous improvement based on it. Vijay *et al.* [22] proposed SegNet, which retains the pooling layer's index during the encoder pooling and maps the value to the initial position accurately according to the index in the decoder. This improvement improves the effect of image segmentation without additional learning. Ronneberger *et al.* [23] proposed U-Net for the segmentation of biological microscope images. It is an asymmetric codec network structure. U-Net also adopts the jump-layer structure of the FCN. However, there is a big difference between the two: U-Net transmits the feature images acquired at the encoding stage to the corresponding decoding stage and fuses the feature images at different locations through connection. Due to U-Net's excellent image processing performance, combined with the development of the attention mechanism model and residual structure model, more and more fusion models have achieved the best performance.

B. DENSE CONNECTION

The Densenet [24] structure extends single-layer feature reuse to multi-layer and uses residual structure to connect each layer with all other layers in a dense convolutional network. Dense Block adopts dense connection inside, and features of the i layer are mapped with those of all previous layers:

$$x_i = H_i\left([x_0, x_1, x_2, L, x_{i-1}]\right) \tag{1}$$

where $[x_0, x_1, x_2, L, x_{i-1}]$ represents the cascade of feature mapping, x_i is the feature output of the ith layer, and H(·) is the combination of nonlinear transformation functions.

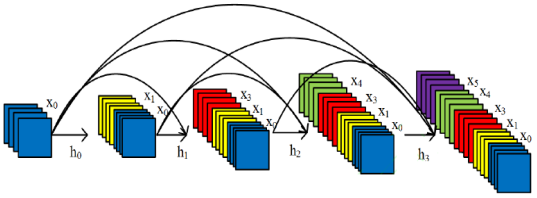

FIGURE 2. Dense block connection.

A typical Dense Block is shown in Fig. 2. On the surface, Densenet differs from ResNet, only using residuals to connect all previous layers. However, this seemingly small change makes the two networks substantially different. Denseness does not need to relearn redundant feature diagrams. This dense connection pattern requires fewer parameters than other structural models. It improves the information flow and gradient across the network, with each layer directly accessing the loss function and raw input—the signal's gradient, which makes training the deep network easier. Besides, dense joining has a regularization effect and reduces overfitting for tasks with a small training set.

C. ATTENTION GATES

Attention Gates are generally used in natural image analysis and language processing (NLP) for machine translation [25] and image classification [26]. Over matrix arithmetic, self-attention mechanisms can apprehend the cooperation between any two positions. As a result, remote dependencies can be modeled without increasing computation and storage costs. A self-attention mechanism has been successfully applied to image modeling [27] and semantic segmentation [28], combined with residual and attention mechanisms to obtain a deep network. RaUnet was obtained by combining residual and attention mechanisms. To focus on the locations associated with impact craters, we take the proposed approach [29] and add a beneficial Attention Gate (AG) to the network architecture, as shown in Fig. 3. The AG inputs are the upsampling function in the augmenting path and the encoder's corresponding segment. The former is used as a gating signal to improve the target area's learning associated with the segmentation task while suppressing the area irrelevant in the mission. Consequently, AG can advance the efficiency of generating semantic information by skip connections. Besides, the activation feature sigmoid is selected to train the convergence of the Gate's parameters and get the attention coefficient α. Then, through multiplying the encoder feature via coefficient α pixel via pixel to get output.

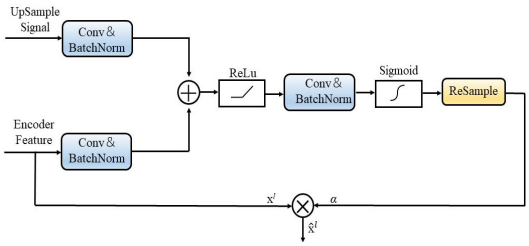

FIGURE 3. Diagram of attention gate.

III. METHODS

In this section, we describe in detail the impact crater extraction process for the NAU-Net. It includes four parts: network structure, loss function, template matching, and evaluation index.

A. NETWORK MODEL

We propose a nested attention-aware segmentation convolutional neural network called NAU-Net. The network combines the strengths of UNet++ and AGs, with a closely supervised encoder-decoder structure and an integrated attention gate skip connection. Besides, mention that NAU-Net introduces an attention mechanism between nested convolution blocks. Features extracted at different craters can be

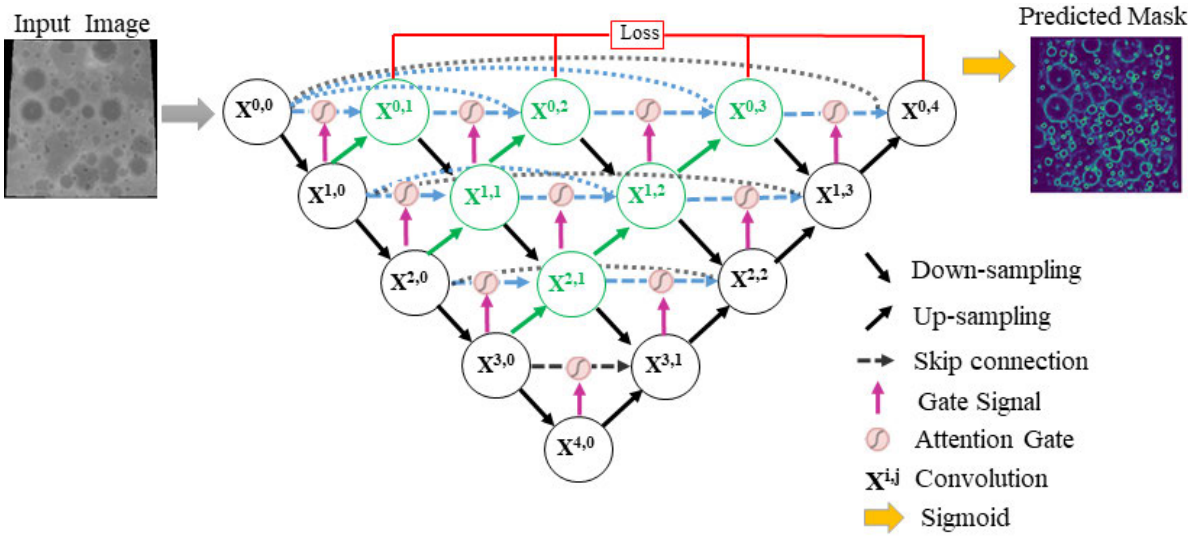

FIGURE 4. Architecture of NAU-Net, based on UNet++. The leftmost map is a 256 × 256 grayscale image sampled from the digital elevation map, and the rightmost the NAU-Net's binary ring mask prediction.

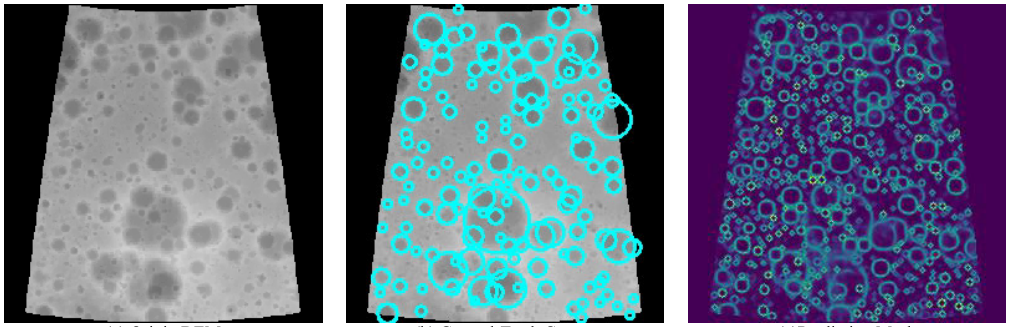

(a) Origin DEM (b) Ground-Truth Craters (c)Prediction Mask

FIGURE 5. Crater prediction result by NAU-Net. (a) A sample Moon DEM. (b) The ground-truth label of lunar images. Yellow circles indicate the ground-truth craters. (c) NAU-Net prediction results.

combined with task-related selections. The network structure of NAU-Net is shown in Fig. 4.

As we can see, NAU-Net consists of an encoder and a decoder, connected by a series of nested dense convolution blocks. Black represents the original U-Net network. Green and blue represent dense convolution blocks on the skip path. The dense connection design Bridges the semantic gap between encoder and decoder feature maps, thus improving the gradient flow. Red indicates in-depth supervision. As described in [29], the green region and backpropagation of the loss function are cut off. Therefore, it is necessary to add a 1 × 1 convolution kernel behind each branch to monitor the convolution block output density. Simultaneously, it can also be $X^{0.1}$, $X^{0.2}$, $X^{0.3}$ final output directly connected, equivalent to the NAU-Net network trim, making the model more flexible. The red, green, and blue components in the figure distinguish NAU-Net from U-Net. Besides, AG can effectively improve the efficiency of propagation of crater feature information through skip connections. After receiving the crater edge feature at each layer, the decoder recovers the feature in a bottom-up manner.

Let $X^{i,j}$ represent the output of node X_i, where i is along with the sampling layer under the encoder index, and j is along with the convolutional layer of dense blocks along with the skip path index. The characteristic graph stack represented by $X^{i,j}$ is calculated as follows:

$$x^{i,j} = \begin{cases} \Theta\left[x^{i-1,j}\right] & j = 0 \\ \Theta\left[\int_{k=0}^{j-1} Ag\left(X^{i,k}\right), Up\left(X^{i+1,j-1}\right)\right] & j > 0 \end{cases} \quad (2)$$

where function $\Theta(\cdot)$ is the convolution operation of the activation function, $U_p()$ representing the up-sampling layer, $A_g()$ means the attention gate selection respectively, [] denotes the connecting layer. The exact analysis of the first skip pathway in NAU-Net is shown in Fig 6.

Notably, the network extracts features from the encoder and transmits them to the decoder via dense skip connections,

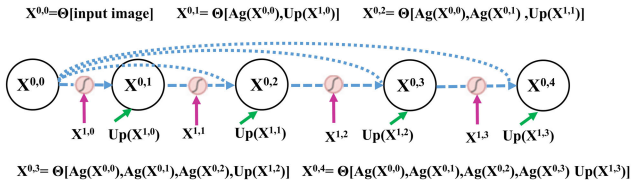

FIGURE 6. Detailed analysis of the first skip pathway of NAU-Net.

represented in an integration hierarchy. The attention gate mechanism is added between the nested convolution blocks. The crater edge features extracted at different levels can be combined with the center selection in the extended path. As a result, the accuracy of NAU-Net is effectively improved.

B. LOSS FUNCTION

To introduce in-depth supervision, NAU-Net introduces the convolution layer and sigmoid function in each output node. The diagram of in-depth supervision is shown in Fig. 7.

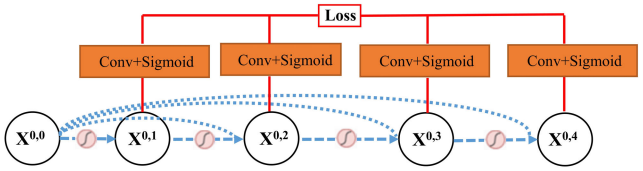

FIGURE 7. Diagram of deep supervision in NAU-Net.

The loss function estimates the inconsistency between the impact crater results predicted by NAU-Net and the truth in machine learning. The loss function estimates the inconsistencies between the predicted results and the truth in machine learning. With the increase of training times, the smaller the function's loss value, the better the robustness of the model. Crater detection is a binary classification issue, which essentially detects whether the pixel is located at the crater's edge. Therefore, the loss function of the NAU-Net training process has adopted the loss of binary cross-entropy (BCE):

$$loss = y_i - y_i t_i + \log(1 + \exp(-y_i)) \tag{3}$$

where y_i is the label of the pixel i in the NAU-Net prediction result and t_i is the label of this pixel in the ground truth. The image loss is the sum of all pixel losses. If the difference between the predicted image and the marked image is large, the loss will be more significant.

C. TEMPLATE MATCHING

The image predicted by the NAU-Net network cannot directly predict the impact crater's specific information, such as the location information of the impact crater, the radius of the impact crater. Most craters are circular. Referring to the template matching algorithm used in [13], an image processing package for matching craters' edges. The detailed process is as follows:

Firstly, in the blank image, the circle with Ra as the radius is used as the template. Besides, the prediction result of the network is used as the target image. After that, the matching template algorithm is used to obtain the matching results. In this algorithm, a matching threshold is set to deal with unreliable matching results. This threshold is 0.5 [20], and the radius Ra is 5-40 km. Due to many overlapping craters, the validity of using Hough transform to detect the ring in the segmentation results is very low. It takes more time than template matching to set a smaller value of center distance. Therefore, the template matching algorithm is more accurate than other methods. In the end, it is critical to decide whether the craters have been efficiently identified after extracting the craters. Given a test lunar image data I, $(\mathrm{x}_i,\mathrm{y}_i)$ is the location of an impact crater extracted from NAU-Net, where x_i is the accuracy of the impact crater and y_i is the latitude of the impact crater. (x_{tj}, y_{tj}) correspond to the real crater location of c_i, where x_{tj} is the latitude of the real crater, y_{tj} is the accuracy of the real crater, and r_j is the real radius of the crater. If the predicted impact crater satisfies (4) and (5), then the detected impact crater is correct. Otherwise, it is the wrong one. $D_{x,y}$ is the longitude and latitude error threshold, and D_r is the radius error threshold. In the experiment, set $\mathrm{D}_{x,y} = 2.0$ $\mathrm{D}_r = 1.0$ [20].

$$\left(\left(x_i - x_{tj}\right)^2 + \left(y_i - y_{tj}\right)^2\right) / \min\left(r_i, r_j\right)^2 < D_{x,y} \tag{4}$$

$$abs(r_i - r_j) / \min(r_i - r_j) < D_r \tag{5}$$

D. EVALUATION METHODS

In general semantic segmentation tasks, IOU is often used as evaluation methods. However, the IOU is not suitable for the craters recognition task because we need to extract the craters from the predicted results. Therefore, the following evaluation methods commonly used in machine learning, with P as accuracy and R as recall rate, are used to evaluate the performance of classification models in machine learning.

$$P = \frac{T_p}{T_p + F_p} \tag{6}$$

$$R = \frac{T_p}{T_P + F_{\mathrm{n}}} \tag{7}$$

where T_p is the total number of impact craters satisfying the equations (6) and (7). In addition to the satisfying craters, those that do not match the actual craters database in the prediction are always marked as newly discovered craters and F_p. The number of unrecognized craters in the real craters database is F_n. $T_p + F_n$ represents the actual number of craters and $T_p + F_p$ represents the predicted number of craters.

Generally, when accuracy is high, recall rates are low, and vice versa. To balance the effect of precision and recall rate. Using F_β to measure classification performance, when recall rate is more important, make $\beta > 1$, when accuracy is more important, let $\beta < 1$, when both are equally important, let $\beta = 1$. F is defined as:

$$F_\beta = \left(1 + \beta^2\right) \times P \times R / \left(\beta^2 \times P + R\right) \tag{8}$$

Due to the incomplete lunar craters database, many actual craters are not marked. Secondly, the training labels provided

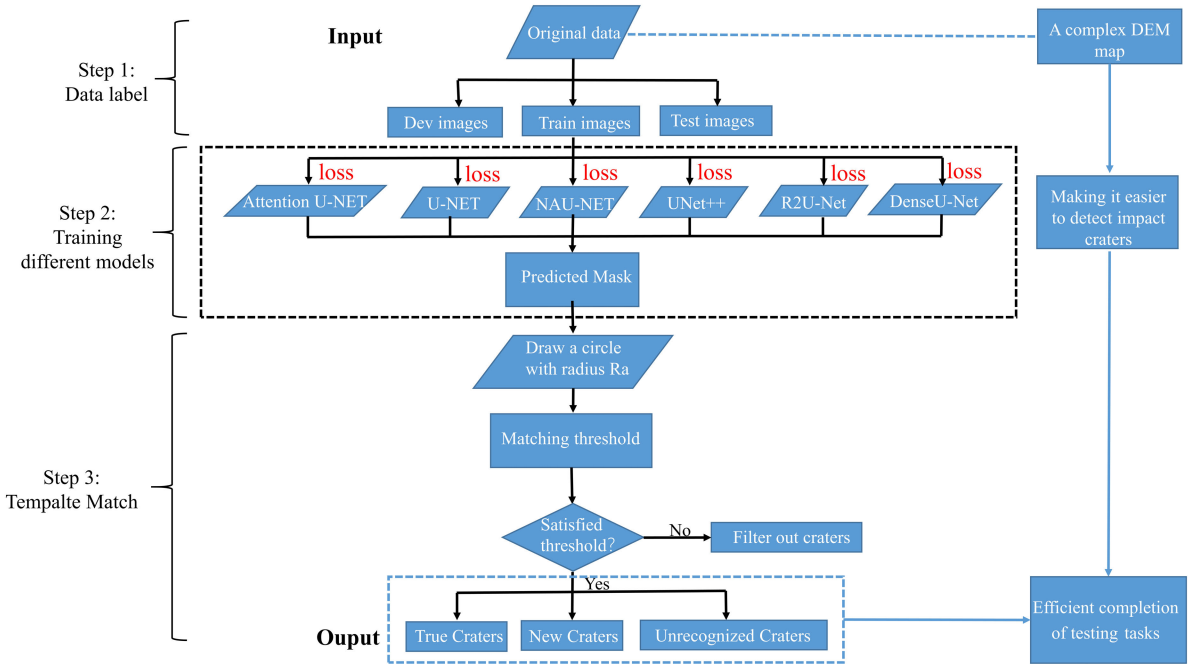

FIGURE 8. Experimental flow chart of impact crater detection.

by Head and Povilaitis are not complete. Therefore, more attention is paid to recall rate indicators, making $\beta = 2$.

Besides, new craters are found in the NAU-Net network, and the index of discovery rate (DR) is increased, including the first discovery rate (DR_1) and the second discovery rate (DR_2). DR_1 is the ratio of the number of newly discovered craters to all accepted craters. DR_2 is the ratio of newly discovered craters to the number of all craters (both identified and unidentified).

Finally, the accuracy of the identified craters' location and radius is added to the performance of the evaluation model. The following formulas are used to calculate the latitude error ($Error_{la}$), longitude error ($Error_{lo}$), and radius error ($Error_r$) of the crater identification.

$$\begin{cases} Error_{la} = abs(la_p - la_t) \times 2/\left(r_p + r_t\right) \\ Error_{lo} = abs(lo_p - lo_t) \times 2/\left(r_p + r_t\right) \\ Error_r = abs(r_p - r_t) \times 2/\left(r_p + r_t\right) \end{cases} \tag{9}$$

where lo_p is the predicted longitude value of meteorite crater, lo_t is the corresponding longitude value of the real meteorite crater. la_p is the predicted meteorite crater latitude value. l_{at} is the corresponding real meteorite crater latitude value. r_p is the predicted meteorite crater's radius, and r_t is the corresponding real meteorite crater radius.

IV. EXPERIMENTAL RESULTS

In this section, we present the detection of NAU-Net on NASA's lunar DEM data [30]. Implementation was made in Keras. Our model is compared with the CNN proposed by UNet [7], DenseUNet [31], Attention UNet [32], UNet++ [29], and R2Unet [33] by modifying the amount of training images.

A. INPUT DATASET

Referring to [7] data, the experimental data in this paper are from the DEM fused by the Lunar Reconnaissance Orbiter (LRO) and the Kaguya probe, with a resolution of 59 m. The reason for using the DEM data set is to avoid the influence of light and perspective on the experimental results. The size of the image is 92160 × 30720 and ranges from 0 to 360 °E and 60 °S to 60 °N. Due to GPU memory limitation, lunar DEM images were cropped to multiple 256 × 256 images. Python Cartopy is used to transform the image into an orthogonal projection to reduce image distortion.

According to the position information of lunar impact craters provided by Head *et al.* [34] and Povilaitis *et al.* [35], a circle was drawn in the blank image of 256 × 256 as the edge label of the impact craters. The total number of impact craters in the Head data set was 5186, with a diameter greater than 20 km. The total number of impact craters in the Povilaitis data set was 19,337 with a diameter of 5-20 km. The validation data set and test data are generated in the same way, and the area of the test image generated is different from the location of the training image, which ensures that the test image is in the training and validation data set.

B. HYPER PARAMETERS SELECTION

In this paper, the depth of three-layer and four-layer neural networks is used for training. The input image size is 256 × 256 × 3, and the final value represents the dimension with the number of channels as 3. For each network depth's

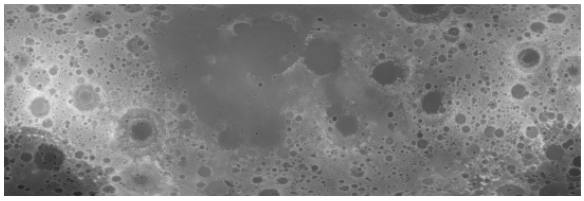

FIGURE 9. The lunar DEM is based on data from the lunar orbiter and Kaguya. (The image resolution is 118m/piex.).

convolutional layer, a 3×3 convolution kernel is adopted, and the Relu activation function is used after each convolution.

In the model parameter setting, each parameter in the network is initialized, and the bias is initialized to 0. In this experiment, the NAU-Net network batch size is set as 10, the network learning rate is specified as 0.0001, the number of model training iterations is set as 20 epochs, the number of filters was set as 112, the length of filters was set as 3, and the dropout is set as 0.15. Keras is used as the deep learning framework, and Tensorflow is used as the back end. The training graphics card is 2 NVIDIA GeForce RTX 2080Ti GPUs, with 64GB memory and Ubuntu 16.04 operating system.

C. NETWORK PERFORMANCE COMPARISON

The number of training images is 30,000. We run each algorithm randomly six times. The number of verified images is 5000. The number of test images is 5000. The meteorite crater identification results of different networks are shown in Fig 10.

TABLE 1. Rececognition results of 30,000 training images by different network models.

Measure	NAU-Net	U-Net++	Attention U-Net	U-Net	R2 U-Net	Dense U-Net
Recall	**0.791109**	0.721778	0.569345	0.761345	0.642593	0.564335
Precision	0.856541	0.809214	0.813611	0.832411	0.848007	**0.870313**
F2-Score	**0.774405**	0.555614	0.592073	0.765073	0.663872	0.595834
DR_1	**0.150575**	0.100827	0.139154	0.139154	0.117717	0.100240
DR_2	0.107748	0.072940	0.117988	**0.117988**	0.104943	0.078598
Error-lo	0.092729	0.094897	0.106109	**0.090109**	0.095057	0.095924
Error-la	**0.082339**	0.097413	0.103450	0.103450	0.095117	0.098287
Error-ra	**0.040178**	0.069064	0.072910	0.072910	0.071082	0.069840

To prove our algorithm's performance, we use the evaluation index to evaluate 5000 test images to evaluate the model after training. The recognition results of each algorithm are shown in Table 1. It offers the mean value of recall rate, accuracy, F2- score, discovery rate, latitude error expressed as Error-lo, longitude error described as Error-la, and radius error as Error-ra. For the first five indicators, a higher measurement value indicates better recognition results, while for the last three indicators, a lower value indicates better recognition performance.

As shown in Table 1, the recall rate and discovery rate of NAU-Net are higher than that of U-Net and UNet++ networks because NAU-Net adds attention mechanism and nested connections, increasing the weight of the target region. Besides, the identification error rate of NAU-Net is lower than that of most networks. The radius error rate is only 4% related to in-depth supervision and can achieve more accurate segmentation. It is worth mentioning that the F2-score of NAU-Net reached 77.4%, which means our network pays more attention to the recall rate. Our network adaptability is better despite the incomplete labeling of the training data set. We can see that, among all the methods compared, our method achieves the best recognition performance overall.

D. SMALL SAMPLE LEARNING COMPARISON

We retrain the network model by changing the number of training images to test the learning ability of NAU-Net. The number of training images is 10000, and our model and other different networks were randomly run five times. The results are shown in Fig 11., which also reports the recall rate, accuracy, F2-Score, network model discovery rate, latitude and longitude error, and radius error averages for each algorithm. It can be concluded from Fig 11. that the accuracy and recall rate of NAU-Net on 10,000 training images is higher than that of other networks. The recall rate of NAU-Net was 0.735, which was about 3% higher than that of UNet++ and 2% higher than that of U-Net. The F2-score of NAU-Net reached 0.751, which was about 4% higher than that of UNet++ and 5% higher than U-Net. Besides, NAU-Net has the lowest error rate of any model. At the same time, it can be found that the recognition result of using 30,000 training data is better than that of using 10,000 images. Our model is more suitable for small data sets.

E. TRAINING BATCHES

In order to test the convergence speed and detection accuracy of our designed model, we set the number of training as 100 and the number of training for each batch as 3000 and draw the curve of loss and accuracy of NAU-Net.

Fig 12. shows the loss and accuracy curves for the training of NAU-Net. It can be seen from Fig 12. that the network reaches 0.05 around 20 epochs, and the convergence speed is fast, which is inseparable from the attention mechanism. Due to the deep supervision method, the released network's training accuracy has been around 0.978, and the effect is satisfactory.

V. DISCUSSION

In this section, we discuss our model from three perspectives. First of all, we analyze the experimental results of NAU-Net. Secondly, the semantic segmentation network model is discussed. Finally, the extraction method of the lunar impact crater is explained.

A. NAU-NET RESULT

We propose a new U-Net image segmentation network with a nested attention mechanism, which achieves good recognition in impact crater recognition. Compared with Sliburt's method [36], our algorithm improved the recognition rate and recall rate by 5% and 4%, respectively. Besides, in

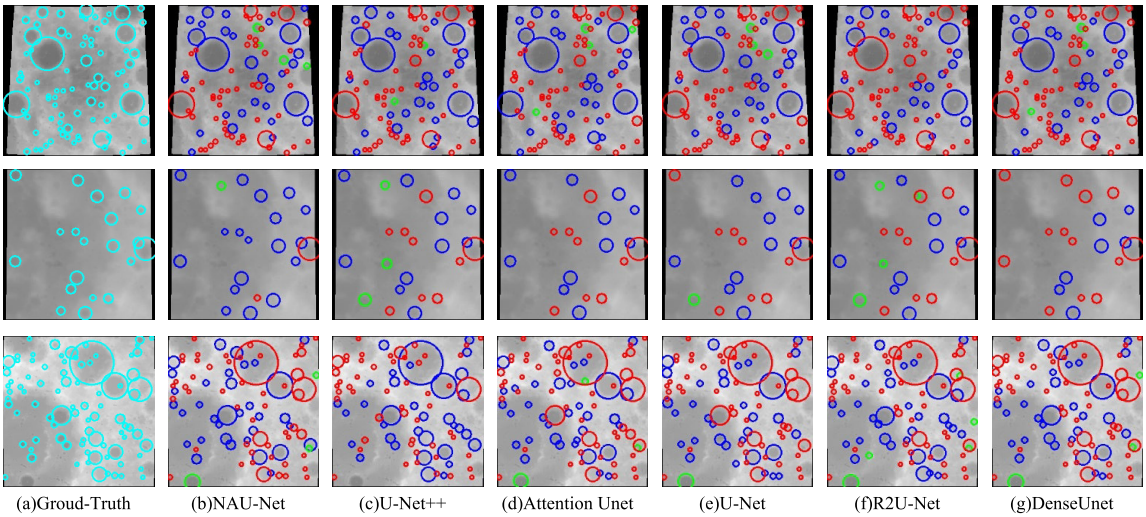

FIGURE 10. Moon crater detection results of different networks. (a) Groud-Truth Craters. (b) NAU-NET. (c) UNet++. (d) Attention U-Net. (e) U-Net. (f) R2U-Net. (g) DenseUnet. New crater predictions are presented in green circles, blue circles denote correctly recognized craters, red circles denote unrecognized craters predicted by the network.

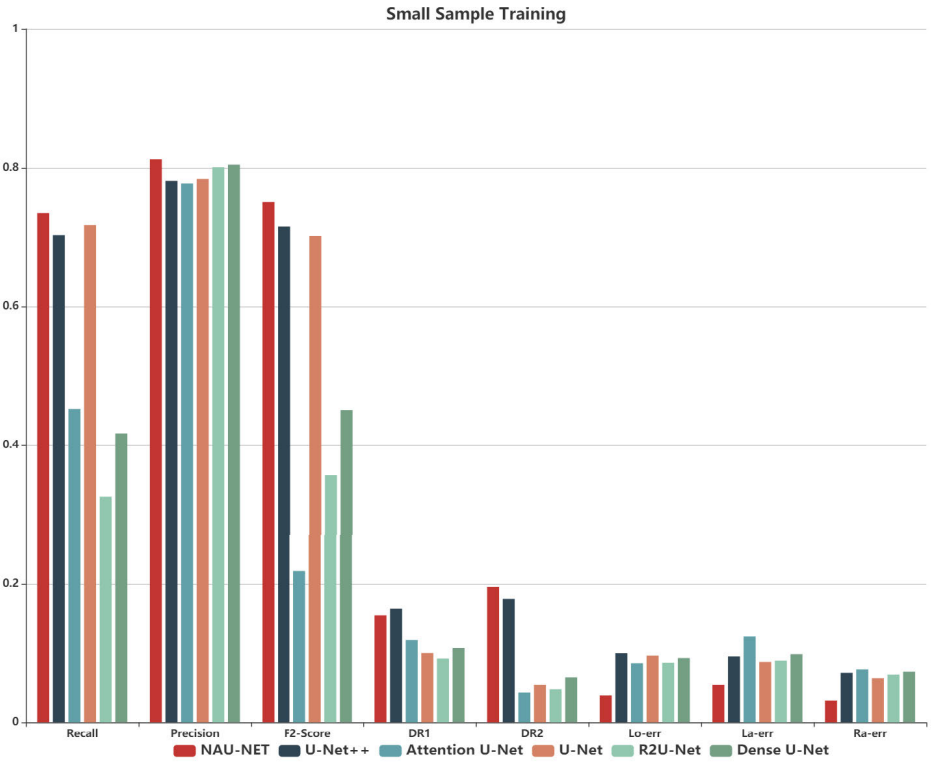

FIGURE 11. The recognition results of 10,000 training images by six network models.

small sample learning, compared with DenseU-Net, Attention UNet [29], UNet++ [30], and R2-UNet [31], NAU-Net has strong learning ability and is suitable for application on small data sets. Our approach is superior to others because it combines the U-Net and Attention Network's advantages with nested, densely connected modules and has better learning capabilities than other networks.

B. IMAGE SEMANTIC SEGMENTATION MODEL

We designed the network to identify impact craters using image segmentation methods to extract the edges of impact craters from lunar digital elevation data. We improve U-Net by using nested dense connection modules, attention mechanisms, in-depth monitoring, and so on. Experiments have shown that our network takes advantage of a redesigned

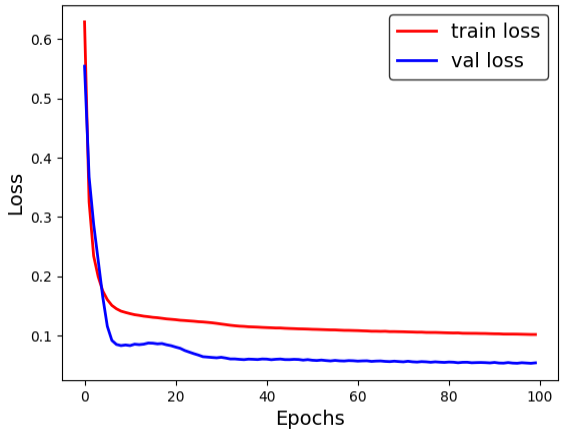

(a) Loss-Epochs

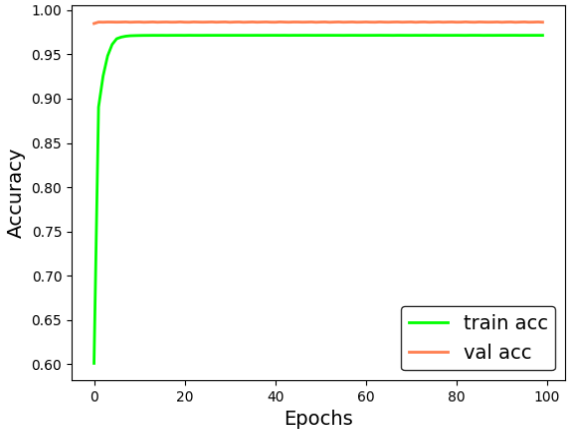

(b) Accuracy-Epochs

FIGURE 12. Loss and accuracy curves of each epoch obtained by NAU-Net.

skipping path and in-depth supervision and Attention Gate. The redesigned skip path is designed to reduce the semantic gap between the feature graph of the encoder and the decoder subnet to bring a more straightforward optimization problem for the optimizer. In-depth supervision can also achieve more accurate segmentation, and Attention Gate can improve the efficiency of propagating semantic information through skip connections. So it solves the problem of gradient disappearance and gradient explosion in a deep convolutional network.

C. IMPACT CRATER EXTRACTION METHOD

This paper uses the template matching algorithm to better extract impact craters from segmentation results than the Canny edge and Hough Transform [20]. It can remove smaller holes from larger craters. Furthermore, we can use smaller thresholds to recognize overlapping craters. However, the Canny edge and Hough transforms are challenging to deal with in these cases. They are appropriate for handling impartial and separate impact craters.

VI. CONCLUSION

In this paper, an efficient and fast impact crater recognition algorithm is proposed to identify impact craters from the lunar digital elevation model. The introduction of nested dense blocks and attention mechanisms can effectively improve the recognition efficiency of the network. The research will help lunar researchers map lunar craters more effectively. We use image semantic segmentation and template matching to solve lunar impact craters density and overlap and propose a new convolutional neural network, namely lunar impact craters recognition network NAU-Net based on U-Net++ and attention mechanism. Experimental results show that this model is practical and feasible to identify impact craters from the lunar digital elevation map. Compared with other image segmentation methods applied to lunar impact craters, this network has better performance parameters and can achieve a better recognition effect. It plays a more prominent role in small sample data.

In future work, we will continue to research three aspects. First, in the image segmentation network, we will apply the instance segmentation method to directly identify an impact crater, such as the MASK-RCNN [36] network. We combine our way with some traditional classification methods, such as the Hough transform, for crater identification on Mars or Mercury. Secondly, in terms of data sources, we may pay more attention to multi-source data fusion, improve accuracy, and combine DEM features and remote sensing image features to identify the way. Finally, we will identify small impact craters (D $<$ 1km) to pave the way for lunar lander landings and navigation applications.

ACKNOWLEDGMENT

The authors would like to thank all reviewers and editors for their comments on this article. They would also like to thank the Space Engineering University for its hardware support and NASA's Lunar digital elevation model data. Finally, they would like to thank Professor Wan Gang from the Space Engineering University for his valuable thoughts.

REFERENCES

[1] R. F. Fudali, "Impact cratering: A geologic process," *J. Geol.*, vol. 97, no. 6, p. 773, Mar. 1989.

[2] G. Neukum, B. Nig, and J. Arkani-Hamed, "A study of lunar impact crater size-distributions," *Moon*, vol. 12, no. 2, pp. 201–229, Feb. 1975.

[3] R. A. Craddock, T. A. Maxwell, and A. D. Howard, "Crater morphometry and modification in the sinus sabaeus and margaritifer sinus regions of mars," *J. Geophys. Res., Planets*, vol. 102, no. E6, pp. 13321–13340, Jun. 1997.

[4] D. De Rosa, B. Bussey, J. T. Cahill, T. Lutz, I. A. Crawford, T. Hackwill, S. van Gasselt, G. Neukum, L. Witte, A. McGovern, P. M. Grindrod, and J. D. Carpenter, "Characterisation of potential landing sites for the European space Agency's lunar lander project," *Planet. Space Sci.*, vol. 74, no. 1, pp. 224–246, Dec. 2012.

[5] J. R. Kim, J.-P. Muller, S. van Gasselt, J. G. Morley, and G. Neukum, "Automated crater detection, a new tool for mars cartography and chronology," *Photogramm. Eng. Remote Sens.*, vol. 71, no. 10, pp. 1205–1217, Oct. 2005.

[6] A. Flores-Méndez, "Crater marking and classification using computer vision," in *Proc. Iberoamerican Congr. Pattern Recognit.*, Nov. 2003, pp. 79–86.

[7] A. Silburt, M. Ali-Dib, C. Zhu, A. Jackson, D. Valencia, Y. Kissin, D. Tamayo, and K. Menou, "Lunar crater identification via deep learning," *Icarus*, vol. 317, pp. 27–38, Jan. 2019.

[8] H. Lee, H.-L. Choi, D. Jung, and S. Choi, "Deep neural network-based landmark selection method for optical navigation on lunar highlands," *IEEE Access*, vol. 8, pp. 99010–99023, 2020.
[9] M. Ali-Dib, K. Menou, A. P. Jackson, C. Zhu, and N. Hammond, "Automated crater shape retrieval using weakly-supervised deep learning," *Icarus*, vol. 345, Sep. 2020, Art. no. 113749.
[10] D. M. DeLatte, S. T. Crites, N. Guttenberg, and T. Yairi, "Automated crater detection algorithms from a machine learning perspective in the convolutional neural network era," *Adv. Space Res.*, vol. 64, no. 8, pp. 1615–1628, Oct. 2019.
[11] G. G. Michael, "Coordinate registration by automated crater recognition," *Planet. Space Sci.*, vol. 51, nos. 9–10, pp. 563–568, Aug. 2003.
[12] A. Fitzgibbon, M. Pilu, and R. B. Fisher, "Direct least square fitting of ellipses," *IEEE Trans. Pattern Anal. Mach. Intell.*, vol. 21, no. 5, pp. 476–480, May 1999.
[13] M. C. Burl, "Automated detection of craters and other geological features," in *Proc. Int. Symp. Artif. Intell. Robot. Automat. Space*, Jun. 2001, pp. 1–8.
[14] N. Harada, T. Hayashi, N. Hirata, H. Demura, and N. Asada, "Recognition algorithm for topographic features," presented at the IEEE Int. Conf. Comput. Inf. Technol., Jul. 2007.
[15] H. Shiozawa, Y. Kanazawa, and K. Kanatani, "Reliability evaluation of conic fitting," *IPSJ SIG Notes*, vol. 1995, pp. 49–56, Feb. 1995.
[16] S. M. Thomas and Y. T. Chan, "A simple approach for the estimation of circular arc center and its radius," *Comput. Vis., Graph., Image Process.*, vol. 45, no. 3, pp. 362–370, Mar. 1989.
[17] T. Vinogradova, M. Burl, and E. Mjolsness, "Training of a crater detection algorithm for Mars crater imagery," in *Proc. IEEE Proc. Aerosp. Conf.*, Jul. 2002, p. 7.
[18] J. P. Cohen and W. Ding, "Crater detection via genetic search methods to reduce image features," *Adv. Space Res.*, vol. 53, no. 12, pp. 1768–1782, Jun. 2014.
[19] W. Fa and Y.-Q. Jin, "A primary analysis of microwave brightness temperature of lunar surface from Chang-E 1 multi-channel radiometer observation and inversion of regolith layer thickness," *Icarus*, vol. 207, no. 2, pp. 605–615, Nov. 2010.
[20] S. Wang, Z. Fan, Z. Li, H. Zhang, and C. Wei, "An effective lunar crater recognition algorithm based on convolutional neural network," *Remote Sens.*, vol. 12, no. 17, p. 2694, Aug. 2020.
[21] J. Long, E. Shelhamer, and T. Darrell, "Fully convolutional networks for semantic segmentation," *IEEE Trans. Pattern Anal. Mach. Intell.*, vol. 39, no. 4, pp. 640–651, 2015.
[22] B. Vijay, K. Alex, and C. Roberto, "SegNet: A deep convolutional encoder-decoder architecture for scene segmentation," *IEEE Trans. Pattern Anal. Mach. Intell.*, vol. 39, no. 12, pp. 2481–2495, May 2017.
[23] O. Ronneberger, P. Fischer, and T. Brox, "U-Net: Convolutional networks for biomedical image segmentation," in *Proc. Int. Conf. Med. Image Comput. Comput.-Assist. Intervent.* Cham, Switzerland: Springer, 2015.
[24] G. Huang, Z. Liu, L. van der Maaten, and K. Q. Weinberger, "Densely connected convolutional networks," 2016, *arXiv:1608.06993*. [Online]. Available: http://arxiv.org/abs/1608.06993
[25] D. Bahdanau, K. Cho, and Y. Bengio, "Neural machine translation by jointly learning to align and translate," *Comput. Sci.*, vol. 33, no. 3, pp. 33–48, Mar. 2014.
[26] P. Rodriguez, D. Velazquez, G. Cucurull, J. M. Gonfaus, F. X. Roca, and J. Gonzalez, "Pay attention to the activations: A modular attention mechanism for fine-grained image recognition," *IEEE Trans. Multimedia*, vol. 22, no. 2, pp. 502–514, Feb. 2020.
[27] P. Appan and J. Sivaswamy, "Retinal image synthesis for CAD development," in *Proc. Int. Conf. Image Anal. Recognit.* Cham, Switzerland: Springer, 2018, pp. 613–621.
[28] J. Fu, J. Liu, H. Tian, Y. Li, Y. Bao, Z. Fang, and H. Lu, "Dual attention network for scene segmentation," in *Proc. IEEE Conf. Comput. Vis. Pattern Recognit. (CVPR)*, Jun. 2020, pp. 3146–3154.
[29] Z. Zhou, M. M. R. Siddiquee, N. Tajbakhsh, and J. Liang, "UNet++: A nested U-Net architecture for medical image segmentation," 2018, *arXiv:1807.10165*. [Online]. Available: http://arxiv.org/abs/1807.10165
[30] D. P. Kingma and J. Ba, "Adam: A method for stochastic optimization," Aug. 2014, *arXiv:1412.6980*. [Online]. Available: https://arxiv.org/abs/1412.6980
[31] X. Yang, X. Li, Y. Ye, X. Zhang, H. Zhang, X. Huang, and B. Zhang, "Road detection via deep residual dense U-Net," in *Proc. Int. Joint Conf. Neural Netw. (IJCNN)*, Jul. 2019, pp. 1–7.
[32] O. Oktay, J. Schlemper, L. Le Folgoc, M. Lee, M. Heinrich, K. Misawa, K. Mori, S. McDonagh, N. Y Hammerla, B. Kainz, B. Glocker, and D. Rueckert, "Attention U-Net: Learning where to look for the pancreas," 2018, *arXiv:1804.03999*. [Online]. Available: http://arxiv.org/abs/1804.03999
[33] M. Z. Alom, C. Yakopcic, T. M. Taha, and V. K. Asari, "Nuclei segmentation with recurrent residual convolutional neural networks based U-Net (R2U-Net)," in *Proc. IEEE Nat. Aerosp. Electron. Conf. (NAECON)*, Jul. 2018, pp. 228–233.
[34] J. W. Head, C. I. Fassett, S. J. Kadish, D. E. Smith, M. T. Zuber, G. A. Neumann, and E. Mazarico, "Global distribution of large lunar craters: Implications for resurfacing and impactor populations," *Science*, vol. 329, no. 5998, pp. 1504–1507, Sep. 2010.
[35] R. Z. Povilaitis, M. S. Robinson, C. H. van der Bogert, H. Hiesinger, H. M. Meyer, and L. R. Ostrach, "Crater density differences: Exploring regional resurfacing, secondary crater populations, and crater saturation equilibrium on the moon," *Planet. Space Sci.*, vol. 162, pp. 41–51, Nov. 2018.
[36] H. Kaiming, G. Georgia, D. Piotr, and G. Ross, "Mask R-CNN," *IEEE Trans. Pattern Anal. Mach. Intell.*, vol. 42, no. 2, pp. 386–397, Jun. 2017.

YUTONG JIA received the B.E. degree in aerospace science and technology from Space Engineering University, Beijing, China, in 2019, where he is currently pursuing the degree with the Information Institute. His main research interests include computer vision, remote sensing image analysis, and deep learning.

LEI LIU was born in Hebei, China, in 1984. He received the M.S. and Ph.D. degrees in remote sensing from Peking University, China, in 2011 and 2018, respectively. He is currently an Associate Professor with Space Engineering University. His research interests include geographic information systems, remote sensing, and computer vision.

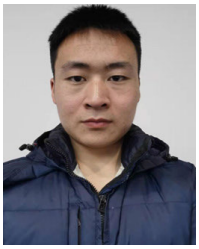

CHENYANG ZHANG received the B.E. degree in TT&C engineering from Space Engineering University, Beijing, China, in 2019, where he is currently pursuing the degree with the Information Institute. His main research interest includes the inversion of water-ice on the poles of the moon.